





Article

Magnetocaloric Properties and Critical Behaviour of the $\text{Sm}_2\text{Ni}_{17}$ Compound

Jihed Horcheni ^{1,2}, Kamal Nouri ³, Hamdi Jaballah ^{1,4} , Lotfi Bessais ^{1,*} , Essebti Dhahri ² 
and Mosbah Jemmali ^{5,6} 

¹ ICMPE, CNRS, University Paris Est Creteil, UMR 7182, 2 Rue Henri Dunant, F-94320 Thiais, France; jihed.horcheni@cnrs.fr (J.H.); hamdi.jaballah@cnrs.fr (H.J.)

² Laboratoire de Physique Appliquée, Faculté des Sciences, Université de Sfax, Sfax 3000, Tunisia

³ Capgemini Engineering, Ile-de-France, Division APA, 12 rue de la Verrerie, 92192 Meudon, France; nourikamel10@yahoo.com

⁴ Lab Mat Org & Propriétés LR99ES17, Faculté des Sciences de Tunis, Université de Tunis El Manar, Tunis 2092, Tunisia

⁵ Faculty of Sciences, University of Sfax, LSME, BP1171, Sfax 3018, Tunisia

⁶ Department of Chemistry, College of Science and Arts, Ar-Rass, Qassim University, P.O. Box 53, Buraydah 51921, Saudi Arabia

* Correspondence: lotfi.bessais@cnrs.fr

Abstract: This paper presents a detailed study in the critical region around the Curie temperature to determine the universality class of the $\text{Sm}_2\text{Ni}_{17}$ intermetallic compound. The magnetocaloric effect has been studied on the basis of experimental measurements of magnetization. Maxwell's relation and a phenomenological model are employed to find the change in magnetic entropy. The compound $\text{Sm}_2\text{Ni}_{17}$ presents a variation in entropy with a moderate maximum and a wide range of operating temperatures. Numerous approaches have been used to explore the spontaneous magnetization behaviour and inverse of the susceptibility, including the modified Arrott technique, the Kouvel–Fisher approach, and the fitting of the critical isotherm. The scaling hypothesis has been used to confirm the validity and interdependence of the critical exponents associated with these phenomena.

Keywords: intermetallics; magnetic phase transition; magnetocaloric effect; phenomenological model; universality class



Citation: Horcheni, J.; Nouri, K.; Jaballah, H.; Bessais, L.; Dhahri, E.; Jemmali, M. Magnetocaloric Properties and Critical Behaviour of the $\text{Sm}_2\text{Ni}_{17}$ Compound. *Appl. Sci.* **2023**, *13*, 6575. <https://doi.org/10.3390/app13116575>

Academic Editor: Roberto Zivieri

Received: 20 April 2023

Revised: 19 May 2023

Accepted: 24 May 2023

Published: 29 May 2023



Copyright: © 2023 by the authors. Licensee MDPI, Basel, Switzerland. This article is an open access article distributed under the terms and conditions of the Creative Commons Attribution (CC BY) license (<https://creativecommons.org/licenses/by/4.0/>).

1. Introduction

Giauque and MacDougall achieved the first experimental demonstration of adiabatic demagnetization of paramagnetic salts, such as $\text{Gd}_2(\text{SO}_4)_3 \cdot 8\text{H}_2\text{O}$, reaching a temperature of 0.25 K [1], after the discovery of the magnetocaloric effect (MCE) by Weiss and Piccard [2] around the Curie temperature (T_C) of Ni. Later, Nikitin et al. [3] reported the largest MCE for $\text{Fe}_{49}\text{Rh}_{51}$. Subsequently, several promising materials, including $\text{Gd}_5(\text{Ge,Si})_4$ [4–7], Fe_2P [8–11], and manganites $\text{R}_{1-x}\text{A}_x\text{MnO}_3$ [12–15], have been extensively studied for their magnetocaloric properties around the ordering temperature (T_C). To this day, the investigation of magnetocaloric materials remains an area of interest for researchers. Recently, several studies have been published showing an interesting magnetocaloric effect over a range of operating temperatures [16–18].

Rare earth (R) and transition metal (M) intermetallics have been thoroughly studied in recent years for their performance as permanent magnets, including $\text{R}_2\text{Fe}_{17-x}\text{M}'_x$ ($\text{M}' = \text{Al, Ga, Si}$) [19], RM_3 [20], R_5M_{19} [21], $\text{RM}_{11}\text{M}'$ ($\text{M}' = \text{Ga, Ti, Co}$) [22], and recently for their magnetocaloric properties, e.g., $\text{La}(\text{Fe,Co,Si})_{13}(\text{H,C})$, R_2Fe_{17} [23–35].

It has been shown that the R_2Ni_{17} systems ($\text{R} = \text{Gd, Tb, Dy, Ho, Er, Tm}$) crystallize in the hexagonal $\text{Th}_2\text{Ni}_{17}$ phase in the $P6_3/mmc$ space group and are ferrimagnetic for a

temperature lower than the Curie temperature (T_C), whereas the $R = Y, Sm$, and Lu compounds are ferromagnetic [36–39]. Nevertheless, In contract to Carfagna and Wallace [36], all Curie temperatures have been found to be lower than 200 K [36–39].

The R_2M_{17} intermetallic compounds have been identified as promising candidates for MCE compounds because of their ease of synthesis and their moderate price. For the binary R_2M_{17} , the substitution of R and/or M has the potential to enhance the modest magnetocaloric effect that characterizes these systems [40–42].

Recently, researchers have focused on the search for new magnetocaloric materials with good low-temperature performance, particularly those exhibiting second-order magnetic transitions (SOMT). SOMT materials are known to have a relatively high cooling capacity, although they typically do not have a very large magnetic entropy change (ΔS_M). Other positive characteristics of SOMT materials include low magnetic hysteresis and an adjustable Curie temperature (T_C) by varying the composition [43,44].

In this work, we have studied the MCE of Sm_2Ni_{17} around T_C . We have derived the MCE, the temperature-averaged entropy change (TEC), and the relative cooling power (RCP). Furthermore, we derived the critical exponent near T_C to determine the universality class of the studied compound.

2. Experiments

The compound Sm_2Ni_{17} was arc-melted several times under a purified argon environment using high-purity elements (Sm (99.98%) and Ni (99.9%)). Afterwards, the ingot produced was enveloped by Ta foil and deposited inside a tube sealed under conditions of 2×10^{-6} bar [45,46]. The ingot was heat-treated for seven days at $T = 1073$ K, followed by water quenching [47,48]. X-ray diffraction (XRD) was performed with a $\theta - 2\theta$ scan geometry between $2\theta = 20$ – 80° using a D8 Brucker diffractometer at 298 K, with $Cu K\alpha$ radiation. The results of X-ray diffraction coupled with Rietveld refinement [49,50] using the Fullprof program [51] are perfectly presented in our work, aiming to establish a ternary phase diagram in Ref. [52]. Isotherms at low temperatures were measured using the Quantum Design PPMS magnetometer with an applied magnetic field ($\mu_0 H_{ext}$) up to 5 T, around T_C , with a step of 2 K. To obtain the internal field, we used $\mu_0 H = \mu_0 H_{ext} - N_d M$, with N_d as the demagnetization constant derived from the M versus $\mu_0 H_{ext}$ plot [53].

3. Results and Discussion

3.1. Structural Properties

Figure 1 shows the XRD and Rietveld analysis for the Sm_2Fe_{17} compound. One can see that the calculated and experimental patterns are in good agreement. The lattice parameters determined from the Rietveld refinement of the XRDs are $a = 8.341(4)$ and $c = 8.062(4)$. This refinement show that the Sm_2Ni_{17} compound crystallizes in the hexagonal Th_2Ni_{17} -type structure of the $P6_3/mmc$ space group.

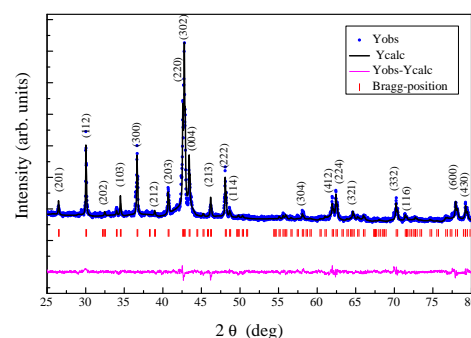


Figure 1. X-ray diffraction and Rietveld refinement of Sm_2Ni_{17} .

The analysis shows that all the peaks are indexed and correspond to Bragg positions of a $P6_3/mmc$ and with no secondary phases. It should be remembered that this arrangement

of CaCu_5 is different from that of $\text{Th}_2\text{Zn}_{17}$ ($R\bar{3}m$), in which dumbbells replace some rare-earth atoms. In this structure, the Ni atoms occupy four crystallographic sites $12k$, $12j$, $6g$, and $4f$, while the Sm atoms occupy two sites, $2c$ and $2b$.

3.2. FM–PM Transition

Figure 2 shows the magnetization versus the temperature using $H = 0.1 \text{ T}$. The $\text{Sm}_2\text{Ni}_{17}$ alloy undergoes a wide ordered–disordered transition. T_C is derived from the extremum of the magnetization derivative (dM/dT) (Figure 2), found to be 160 K. The obtained T_C is comparatively lower than that observed in pure nickel. In rare-earth transition metal compounds, T_C is linked to the exchange interaction. The strength of this interaction is influenced by the distance of the magnetic moment. From the evolution of the hyperfine field versus temperature for $\text{Sm}_2\text{Fe}_{17}$, Morrish et al. [54] deduced that the exchange interaction integrals, for each Fe site, depend on the interatomic iron–iron distances. They observed both negative and positive interactions in $\text{Sm}_2\text{Fe}_{17}$. As the distance between the iron pairs increased, the amplitude of the exchange integrals increased significantly, resulting in a higher Curie temperature. Conversely, decreasing the distance lowered the Curie temperature. Therefore, the low T_C in R_2M_{17} compounds is mainly due to negative exchange interactions.

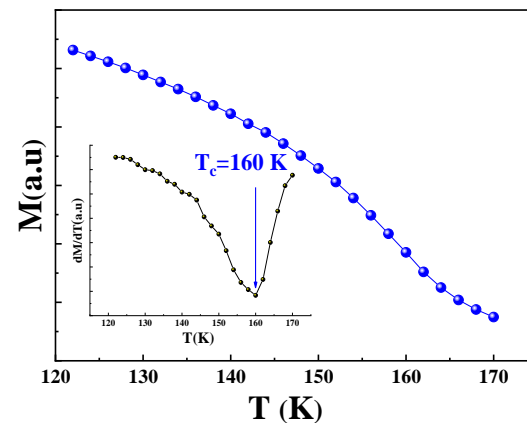


Figure 2. Variation in M versus T at 0.1 T for the $\text{Sm}_2\text{Ni}_{17}$ alloy. The inset is the dM/dT versus T plot.

Figure 3 shows the magnetization (M) plotted as a function of the magnetic field $\mu_0 H$ (0–5 T) at temperatures between 120 and 170 K with a step of 2 K. We clearly obtain an FM state for $T < T_C$ and a PM state for $T > T_C$.

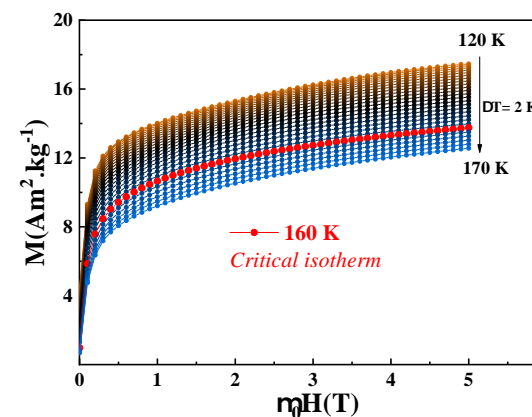


Figure 3. Magnetization versus $\mu_0 H$ (0–5 T) with temperatures ranging from 120 to 170 K for $\text{Sm}_2\text{Ni}_{17}$.

3.3. Magnetocaloric Properties of $\text{Sm}_2\text{Ni}_{17}$

When a magnetic material is under an applied magnetic field, its temperature is affected, this phenomenon is called the MCE. Calculating the change in magnetic entropy

(ΔS_M) is important to study the magnetocaloric effect because it provides a quantitative measure of the effect's magnitude in a given material, which is essential for optimizing the design and performance of magnetocaloric devices for refrigeration and energy conversion applications. The integration of the Maxwell relation is used to calculate the change in magnetic entropy that occurs as a result of the application of a magnetic field:

$$\Delta S_M = \mu_0 \int_0^H \left(\frac{\partial M}{\partial T} \right)_H dH$$

From the experimental measurements $M(H)$ (Figure 3), we derive ΔS_M versus temperature using the following expression [55]:

$$|\Delta S_M| = \mu_0 \sum_i \frac{M_i - M_{i+1}}{T_{i+1} - T_i} \Delta H_i$$

where M_{i+1} and M_i refer to the magnetization at T_{i+1} and T_i , respectively under an increased ΔH_i .

Figure 4 shows the magnetic entropy variation as a function of temperature and the applied magnetic field, especially near the FM–PM transition. It is obvious that the maximum ΔS_M occurs near the Curie temperature, with the peak value heavily reliant on the strength of the magnetic field. Although the maximum ΔS_M is moderate for the studied compounds, the width at mid-height is relatively large ~ 45 K for $\mu_0 H = 5$ T.

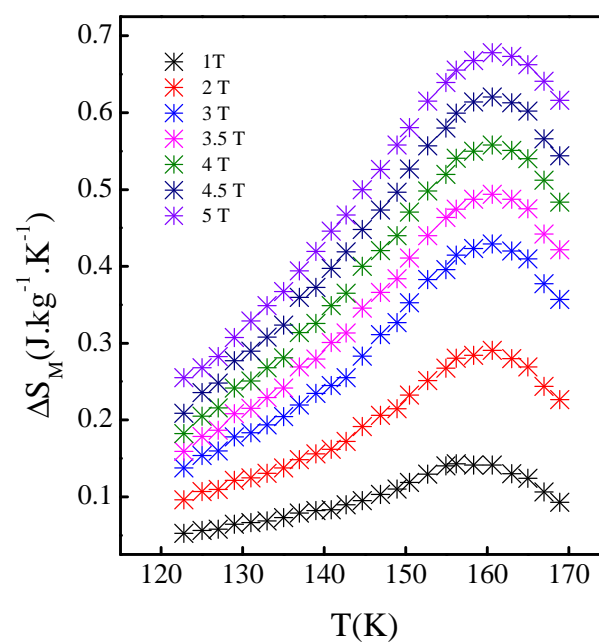


Figure 4. ΔS_M versus temperature for $\text{Sm}_2\text{Ni}_{17}$ with different applied $\mu_0 H$. $|\Delta S_M|$ curves are deduced from magnetic isotherms using the Maxwell relation.

The graphical method commonly used to determine magnetocaloric parameters, such as the magnetic entropy maximum (ΔS_M^{max}), width at half-maximum (δT^{FWHM}), and temperature-averaged entropy change (TEC), are generally not precise enough. Therefore, in the following section, we use a phenomenological model that allows for more accurate estimates of these parameters. In particular, this model allows for the prediction of a material's magnetocaloric effect from a single thermomagnetic measurement at low-applied magnetic fields, thus enhancing its utility.

A phenomenological model is used to simulate the relationship between magnetization and temperature. This simulation is performed assuming adiabatic conditions, under an applied magnetic field, and the model is tuned to closely match the experimental data.

The relationship between magnetization, temperature changes, and T_C can be described as follows [56]:

$$M(T) = \frac{(M_F - M_P)}{2} \tanh[\alpha(T_C - T)] + T \cdot \frac{dM}{dT} \Big|_{T < T_C} + \beta \quad (1)$$

The parameters α and β can be determined using the following equations:

$$\alpha = \frac{2(\frac{dM}{dT} \Big|_{T < T_C} - \frac{dM}{dT} \Big|_{T_C})}{M_F - M_P}$$

$$\beta = \frac{M_F + M_P}{2} - \frac{dM}{dT} \Big|_{T < T_C} \cdot T_C$$

where M_F represents the initial magnetization value around T_C and M_P represents the final magnetization value at the same transition.

In Figure 5, it is evident that the magnetization variations in $\text{Sm}_2\text{Ni}_{17}$, as modelled and measured against temperature, show strong agreement. The experimental data are represented by (*) in the figure, while the simulated magnetization is shown by the red line.

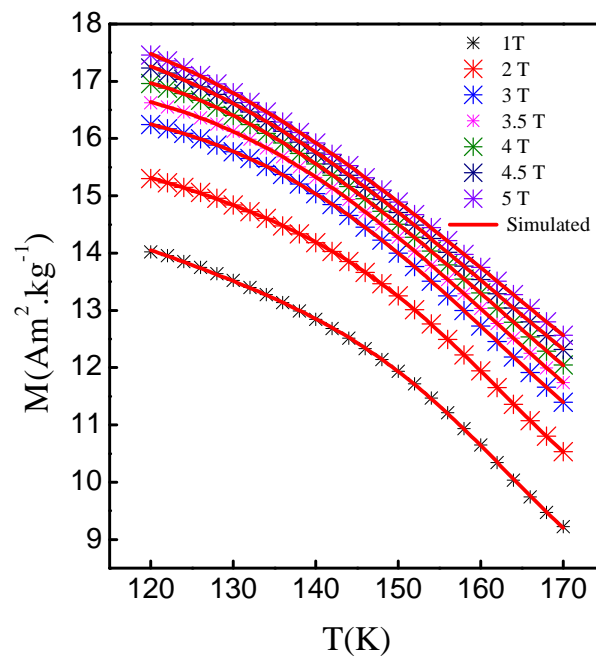


Figure 5. Modelled and experimental magnetization measured under several $\mu_0 H$ plotted against temperature for $\text{Sm}_2\text{Ni}_{17}$.

The magnetization sensitivity in the ordered magnetic state is represented by $\frac{dM}{dT} \Big|_{T < T_C}$, while at T_C it is denoted by $\frac{dM}{dT} \Big|_{T_C}$.

To obtain ΔS_M of a compound undergoing adiabatic variation of the external magnetic excitation from 0 to a final value of the internal magnetic field ($\mu_0 H_{max}$), the following equation can be used :

$$\Delta S_M = -\alpha \cdot \mu_0 H_{max} \frac{M_F - M_P}{2} \text{sech}^2[(\alpha(T_C - T))] + \left(\frac{dM}{dT} \Big|_{T < T_C} \right) \cdot \mu_0 H_{max} \quad (2)$$

Equation (2) indicates that a large observed ΔS_M is due to the presence of high magnetization for $T < T_C$ and a rapid decrease in magnetization for $T = T_C$. Therefore, the maxi-

imum value of ΔS_M , denoted as ΔS_M^{max} , can be derived using Equation (2). At $T = T_C$, ΔS_M is equivalent to ΔS_M^{max} , expressed as follows:

$$\Delta S_M^{max} = (-\alpha \frac{(M_F - M_P)}{2} + (\frac{dM}{dT}|_{T < T_C})) \mu_0 H_{max}$$

Furthermore, the determination of the half-value width, δT^{FWHM} , of ΔS_M can be determined using the following approach:

$$\delta T^{FWHM} = \frac{\alpha}{2} \operatorname{acsh}[(\frac{2\alpha(M_F - M_P)}{2(\frac{dM}{dT}|_{T_C}) + \alpha(M_F - M_P)})^{1/2}]$$

The relative cooling power (*RCP*) is a crucial parameter in the application of magnetocaloric materials, which is related to ΔS_M^{max} and FWHM for the variation in ΔS_M with temperature, as stated in [24].

The expression for *RCP* is given by the following equation:

$$RCP = \Delta S_M^{max} \cdot \delta T^{FWHM} = (-\alpha \frac{(M_F - M_P)}{2} + \frac{dM}{dT}|_{T < T_C}) \times \frac{\alpha}{2} \operatorname{acsh}[(\frac{2\alpha(M_F - M_P)}{2\frac{dM}{dT}|_{T < T_C} + \alpha(M_F - M_P)})^{1/2}] \mu_0 H_{max} \quad (3)$$

Using the phenomenological model, it is possible to calculate key parameters such as δT^{FWHM} , ΔS_M^{max} and *RCP* for $\text{Sm}_2\text{Ni}_{17}$ compounds while considering variations in the applied magnetic field.

Another important parameter, known as the temperature-averaged entropy change (*TEC*), has been used in addition to *RCP* to evaluate the suitability of materials for magnetic refrigeration applications. Introduced by L. D. Griffith et al. in [57], *TEC* can be computed from the magnetic entropy change data according to the following expression:

$$TEC = \frac{1}{\Delta T_{H-C}} \max \left\{ \int_{T_{mid} - \frac{\Delta T_{H-C}}{2}}^{T_{mid} + \frac{\Delta T_{H-C}}{2}} |\Delta S_M(T)| dT \right\}$$

ΔT_{H-C} is the temperature range of the measurement apparatus and reflects the difference between hot and cold heat exchangers. T_{mid} is the temperature at the centre of ΔT_{H-C} where *TEC* is maximized.

The magnetic entropy variation obtained from the phenomenological model and Maxwell's relation for different applied magnetic fields is compared in Figure 6a. The agreement between the experimental and simulated curves is obvious. This suggests that the phenomenological model is a reliable tool for evaluating the magnetocaloric effect. Moreover, this model can predict the ΔS_M curve based on a magnetization curve measured under a single low magnetic field value, saving time and cost in the measurement process.

In Table 1, we compare the maximum entropy variation values with the *RCP* values for different magnetocaloric intermetallic materials. The $\text{Sm}_2\text{Ni}_{17}$ compound studied in this work exhibits a ΔS_{max} of $0.7 \text{ J}(\text{kg} \cdot \text{K})^{-1}$ and a relatively large mean height width of 45 K. The product of these values yields an *RCP* of $37 \text{ J} \cdot \text{kg}^{-1}$. This is comparable with $\text{Pr}(\text{Co}, \text{Cu})_5$ calculated around the spin reorientation temperature, higher than $\text{Er}_2\text{Ni}_{17}$, SmNi_5 , Pr_2Co_7 , PrCo_{19} , $\text{Fe}_{65}\text{Ni}_{35}$, and GdFe_2 . However, it is approximately four times lower than the PrCo_2Cu_3 compound.

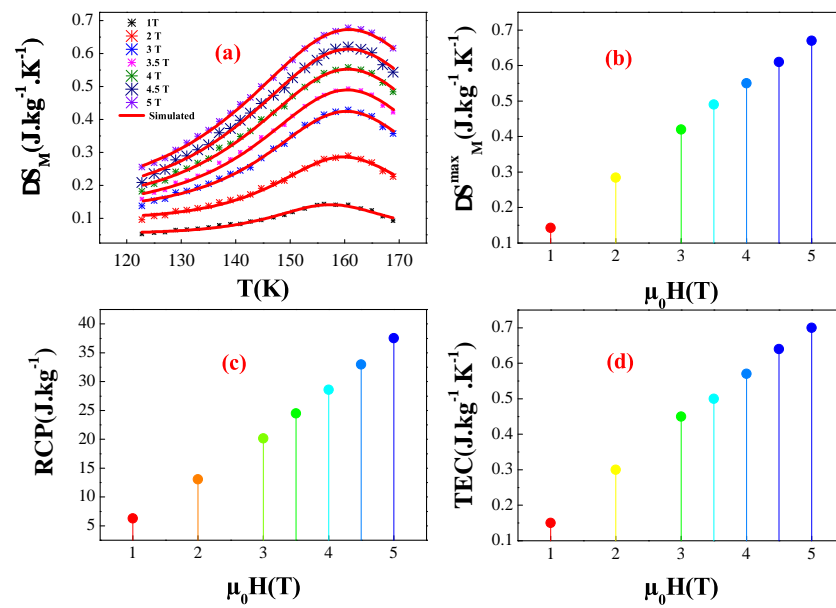


Figure 6. (a) Experimental and simulated magnetic entropy change versus temperature for Sm₂Ni₁₇ under several magnetic fields. (b) Maximum magnetic entropy change plotted against the applied magnetic field. (c) Relative cooling power plotted against applied magnetic field. (d) Temperature-averaged entropy change versus applied magnetic field for $\Delta T_{H-C} = 5$ K.

Table 1. Comparison of RCP and ΔS_{\max} of Sm₂Ni₁₇ and other materials.

Compound	$\mu_0 \Delta H$ (T)	ΔS_{\max} J(K.kg) ⁻¹	RCP J.kg ⁻¹	Ref.
Sm ₂ Ni ₁₇	5	0.7	~37	This Work
Er ₂ Ni ₁₇	5	~0.6	~24	[39]
SmNi ₅	5	5	26.85	[58]
Pr ₂ Co ₇	1.5	1.1	18.5	[59]
Pr ₅ Co ₁₉	1.5	5	18.2	[60]
Fe ₆₅ Ni ₃₅	3	0.35	~18	[61]
Gd ₂ Fe ₂	1.5	0.79	13.3	[62]
PrCo ₂ Cu ₃	4	0.7	~128	[63]

3.4. Critical Phenomenon and Spin Interaction

3.4.1. Arrott Plot

The characteristics of the FM–PM transition in this sample were evaluated using the Arrott plots. Figure 7 displays the Arrott plots obtained from the $M(\mu_0 H)$ curves by plotting the squared magnetization (M^2) against $\mu_0 H / M$. Based on the Banerjee criterion [64], if the Arrott plot slope of the linear curve near the Curie temperature is negative, the FM–PM transition is a first-order magnetic (FOM) transition; conversely, a second-order magnetic transition occurs when the plot has a positive slope. Therefore, the Arrott plots of the Sm₂Ni₁₇ alloy imply an SOMET. The Arrott plot method is utilized to derive the critical exponents and the Curie temperature, assuming $\gamma = 1.0$ and $\beta = 0.5$. This case corresponds to the mean-field model (MFM) critical exponents. The proposed method has been widely explained in the literature [65], involving plotting M^2 versus $\mu_0 H / M$ in the high-field zone exhibiting linear behaviour, and at T_C , where the isotherm is a line intersecting the origin. In contrast, the high magnetic field curves for the Sm₂Ni₁₇ compound shown in Figure 7 do not exhibit parallel behaviour near the transition temperature. This finding indicates that the MFM is inadequate to describe the magnetic phase transition of our compound; therefore, to identify the universality class of the studied compound we use a method based on modified Arrott plots (MAP).

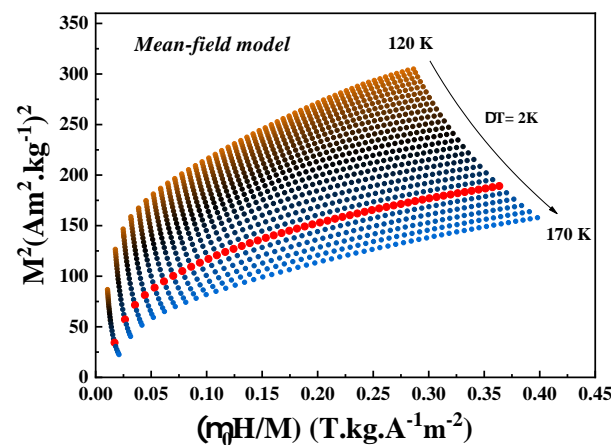


Figure 7. Arrott plots for M^2 versus $\mu_0 H/M$ for temperature ranging from 120 to 170 K with $\Delta T = 2$ K.

To examine other possible exponent pairs (β and γ) the generalized Arrott equation must be used [66].

To determine the appropriate model to describe this phase transition we will use the γ and β couples of the three-dimensional theoretical model commonly used in the literature, such as the tricritical-MFM ($\beta = 0.25$ and $\gamma = 1.0$, Figure 8a), the three-dimensional Ising model ($\beta = 0.325$ and $\gamma = 1.241$, Figure 8b), the three-dimensional Heisenberg model ($\beta = 0.365$ and $\gamma = 1.386$, Figure 8c) and the three-dimensional XY model ($\beta = 0.345$ and $\gamma = 1.316$, Figure 8d) to make the MAPs ($M^{1/\beta}$) versus $(\mu_0 H/M)^{1/\gamma}$.

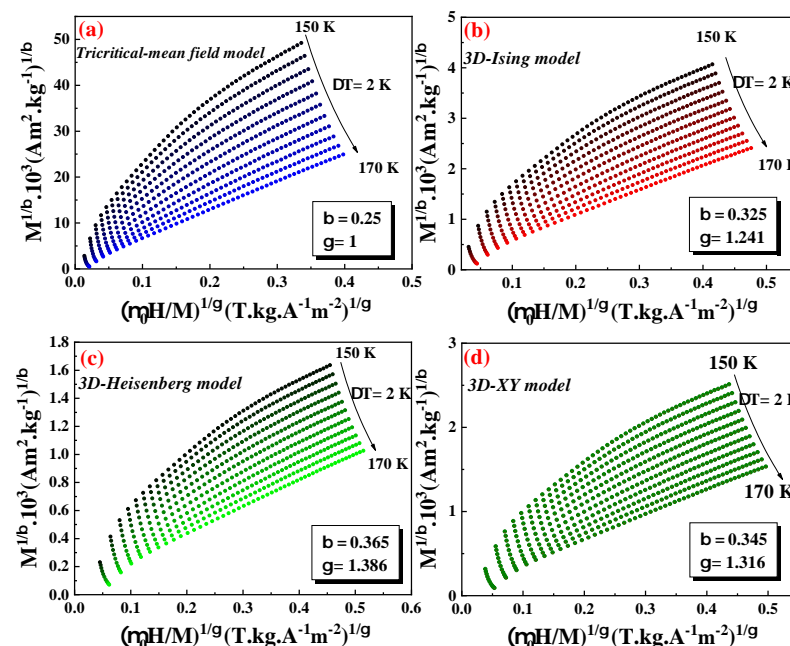


Figure 8. The modified Arrott plots (MAP) of $M^{1/\beta}$ against $(\mu_0 H/M)^{1/\gamma}$, with various exponent pairs (β and γ).

None of the above universality classes seem suitable to directly describe the critical properties of our compound. Since we are dealing with a problem that has two parameters, we employ a method that involves performing multiple iterations, as described below: In the high field data in the three-dimensional Heisenberg model, the initial values of $M_S(T)$ and $\chi_0^{-1}(T)$ are determined by linear extrapolation, where $M_S(T)$ and $\chi_0^{-1}(T)$ are the Y and X intercepts, respectively.

By fitting the data according to Equations (4) and (5) [67], we obtain a set of γ and β values.

$$M_S(T) = M_0(-\varepsilon)^\beta; \quad \varepsilon < 0, \quad T < T_C \quad (4)$$

$$\chi_0^{-1}(T) = \left(\frac{h_0}{M_0}\right)\varepsilon^\gamma; \quad \varepsilon > 0, \quad T > T_C \quad (5)$$

where $\varepsilon = (T - T_C)/T_C$ is the reduced temperature, while the critical amplitudes are represented by $M_S(T)$ and $\chi_0^{-1}(T)$ for spontaneous magnetization and the inverse susceptibility, respectively.

To rebuild a new modified Arrott plot, we employed the derived γ and β . As a consequence, a new γ and β pair are obtained from the deduced $\chi_0^{-1}(T)$ and $M_S(T)$, until the iterations converge and the derived γ and β yield stable values [65]. Using the final values of $\chi_0^{-1}(T)$ and $M_S(T)$ (Figure 9), Equation (4) gives $\beta = 0.26(1)$ and $T_C = 160.6(1)$ K, and Equation (5) gives $\gamma = 1.38(1)$ and $T_C = 159.7(4)$ K.

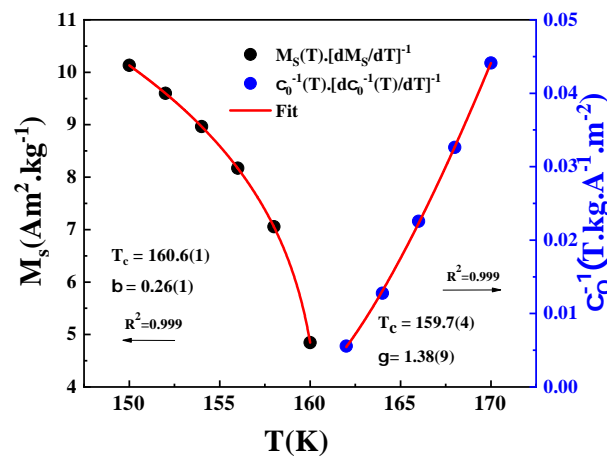


Figure 9. (left) The spontaneous magnetization versus temperature and (right) the inverse of initial susceptibility versus temperature. The solid lines represent the fit.

3.4.2. Kouvel–Fisher Plot

We have utilized the Kouvel–Fisher (KF) technique as our next approach in order to derive more precise sets of T_C , γ , and β in the scaling analysis. The functions employed in this method are described by the following two equations [68]:

$$M_S(T) \left(\frac{dM_S(T)}{dT} \right)^{-1} = \frac{T - T_C}{\beta} \quad (6)$$

$$\chi_0^{-1}(T) \left(\frac{d\chi_0^{-1}(T)}{dT} \right)^{-1} = \frac{T - T_C}{\gamma} \quad (7)$$

By applying the KF approach, $M_S(T) \left(\frac{dM_S(T)}{dT} \right)^{-1}$ and $\chi_0^{-1}(T) \left(\frac{d\chi_0^{-1}(T)}{dT} \right)^{-1}$ exhibit linear behaviour as a function of T , with slopes $1/\beta$ and $1/\gamma$, respectively. The linear fitting shown in Figure 10 using Equation (6) provides $T_C = 160.5(2)$ K and $\beta = 0.25(1)$. In the same way, Equation (7) gives $T_C = 159.7(3)$ K and $\gamma = 1.39(6)$, which is in agreement with those obtained from the MAP. In Table 2, we have summarized the critical exponents of $\text{Sm}_2\text{Ni}_{17}$ and those corresponding to the well-known universality classes. One can see that T_C and the critical exponent's values derived using the KF method are in agreement with those derived utilizing the MAP. This implies that the obtained values are consistent and unequivocal. The final critical exponents, obtained through the KF method, were used to plot the final Arrott plots shown in Figure 11.

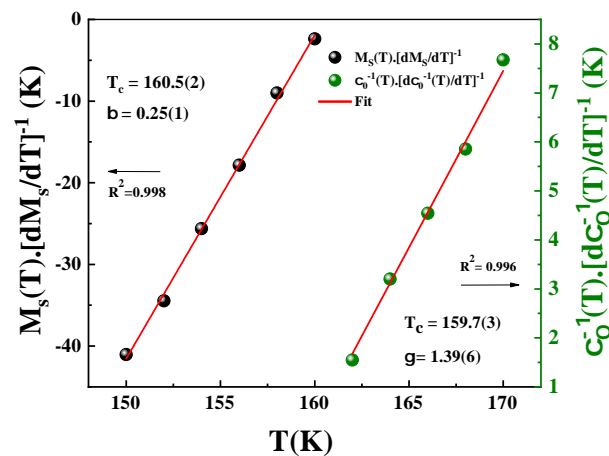


Figure 10. The Kouvel–Fisher (KF) plot displays the temperature-dependent behaviour of spontaneous magnetization $M_s(T, 0)$ and the inverse of susceptibility $\chi_0^{-1}(T, 0)$, plotted against temperature.

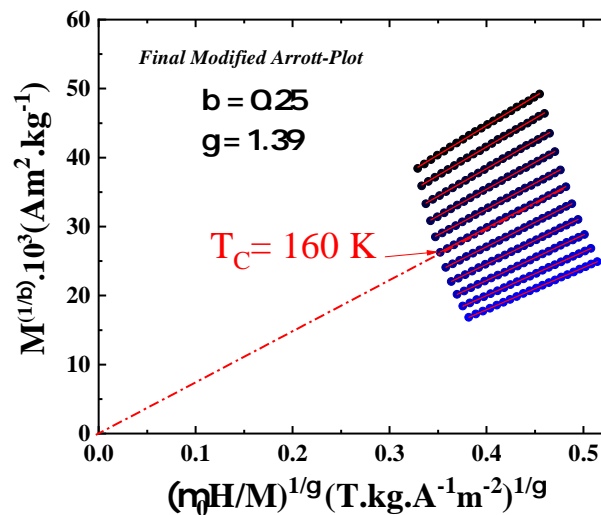


Figure 11. The final MAP using critical exponents, obtained through the KF method.

The resulting plot revealed a series of parallel lines in the strong field region and confirmed the critical isotherm passing through the origin. These observations provide visual confirmation of the validity of the critical exponents. However, to further verify the accuracy of the β and γ values, a method based on the scaling equation is employed at the end of this section.

The determination of the third critical exponent δ involves critical isotherm analysis, requiring the magnetization $M(\mu_0 H)$ at $T_c = 160$ K as $\ln(M)$ versus $\ln(\mu_0 H)$ to be plotted, as illustrated in Figure 12. The equation relating M and $\mu_0 H$ at $T = T_c$ is [69]:

$$\ln(M) = \ln(D) + \frac{1}{\delta} \ln(\mu_0 H) \quad (8)$$

where D is the amplitude and the exponent δ describes the curvature of $M(\mu_0 H)$ at T_c . Based on Equation (8), a linear line with a slope of $1/\delta$ can be derived through linear regression of $\ln(M)$ as a function of $\ln(H)$ at the critical temperature. As depicted in the inset of Figure 12, our analysis using this method yielded a value of $\delta = 6.64(2)$. By applying the Widom scaling equation ($\delta = \frac{\gamma}{\beta} + 1$) [70], with β and γ derived from the KF and MAP plot, $\delta = 6.50(4)$ and $6.36(6)$ was obtained, respectively. These values are consistent with the critical isothermal analysis, demonstrating that the critical exponents obtained are both precise and dependable within the bounds of experimental precision.

Finally, the two methods give values close to δ justifying the validity of this value and confirming that the FM–PM phase transition does not belong to any universality class.

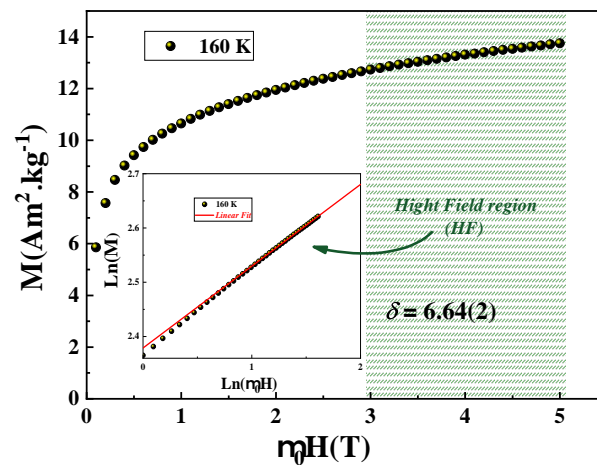


Figure 12. The critical isothermal magnetization curve against the applied magnetic field. The inset shows the same plot in ln–ln scale.

Table 2. The obtained critical exponents of $\text{Sm}_2\text{Ni}_{17}$ (our work) compared to those obtained for comparable materials and those corresponding to the main universality classes.

Composition	Technique	$\langle T_C \rangle$ (K)	β	γ	δ	Ref.
$\text{Sm}_2\text{Ni}_{17}$	MAP	160.6(1)	0.26(1)	1.38(9)	6.36(6)	Our Work
	KF	160.5(2)	0.25(1)	1.39(6)	6.50(4)	
	CI	160			6.64(2)	
Mean-field	Theory	-	0.5	1	3	[71]
3D Heisenberg	Theory	-	0.37(1)	1.39(1)	4.80(4)	[71]
3D Ising	Theory	-	0.33(1)	1.24(1)	4.82(2)	[71]
3D XY	Theory	-	0.35	1.32	4.81	[71]
Tricritical mean-field	Theory	-	0.25	1	5	[71]
$\text{Pr}_2\text{Fe}_{16}\text{Al}$	MAP	357.5	0.37(1)	1.34(1)	4.62(3)	[72]
	KF	358.1	0.37(1)	1.35(1)	4.67(1)	
	CI	358			4.72(2)	
$\text{SmNi}_{2.2}\text{Fe}_{0.8}$	MAP	239.5	0.38(1)	1.30(1)	4.45(4)	[73]
	KF	239.8	0.38(1)	1.30(1)	4.43(8)	
	CI	239			4.63(3)	
$\text{CeCo}_{12}\text{B}_6$	MAP	128	0.39(1)	1.39(1)	4.60	[74]
	KF	128	0.37(1)	1.38(1)	4.77	

It is crucial to check if the obtained T_C and critical exponents produce a scaling equation of state for the system. The magnetic equation of state is stated under the scaling assumption in the asymptotic critical area as follows:

$$M(H, \varepsilon) = \varepsilon^\beta f_\pm(H/\varepsilon^{\beta+\gamma}) \quad (9)$$

where f_- for $T < T_C$ and f_+ for $T > T_C$ are regular analytic functions.

By utilizing the β and γ obtained through the KF method, we plotted the scaled quantity $M/|\varepsilon|^\beta$ as a function of $\mu_0 H/|\varepsilon|^{\beta+\gamma}$, as shown in Figure 13.

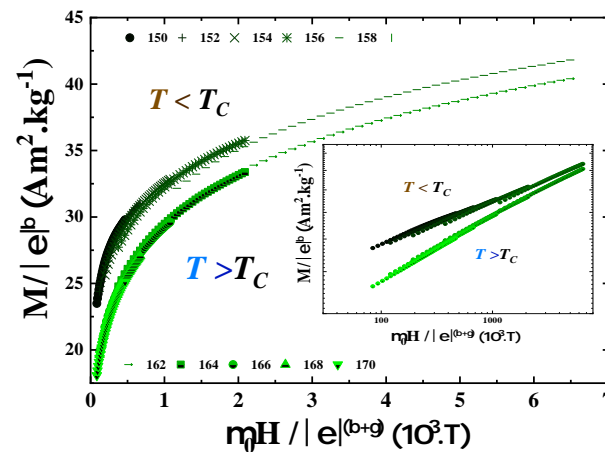


Figure 13. Scaling plots above and below T_C for the $\text{Sm}_2\text{Ni}_{17}$ alloy. The inset shows the same plot in the ln-ln scale.

The resulting graph shows the collapse of all data into two distinct strands below and above the critical temperature T_C . This observation is compelling evidence of our research findings' reliability and robustness. The critical coefficients of our compound obtained in this work together with the theoretical models are compared in Table 2. It can be seen that the experimentally generated coefficients cannot be listed in any of the conventional universality class. The exponent β converges towards the value predicted by the tricritical MFM, while γ exhibits proximity to the value anticipated by the 3D Heisenberg model.

3.4.3. Spin Interaction

Comprehending the interaction range and characteristics of this material is crucial. The universality class of the magnetic phase transition in a homogeneous magnet is determined by $J(r)$, the exchange interaction. Based on analysis of the re-normalization group theory, $J(r)$ is expected to decline as the distance increases, and specifically, it follows a pattern of $J(r) = r^{-(d+\sigma)}$. In this formula d stands for the dimension of the system. At the same time, σ represents the scope or extent of the interaction, and it is known to be greater than zero [75]. In addition, Fisher et al. suggested that the range of σ and γ meet the re-normalization group approach as follows [76]:

$$\gamma = 1 + \frac{4n+2}{dn+8}\Delta\sigma + \frac{8(n+2)(n-4)}{d^2(n+8)^2} * \left[1 + \frac{2G\left(\frac{d}{2}\right)(7n+20)}{(n-4)(n+8)} \right] \Delta\sigma^2 \quad (10)$$

where n is the dimension of the spin and $\Delta\sigma = \left(\sigma - \frac{d}{2}\right)$ and $G\left(\frac{d}{2}\right) = 3 - \left(\frac{1}{4}\right)\left(\frac{d}{2}\right)^2$.

As per this model, the extent of the spin interaction is contingent upon the value of (σ) , indicating whether it is long- or short-ranged, where in a 3D isotropic system, if $\sigma \geq 2$, $J(r)$ may decline quicker than r^{-5} with short-range spin interactions. Whereas if $\sigma \leq 3/2$, $J(r)$ decays more slowly than $r^{-4.5}$ with long-range spin interactions; thus, the MFM is the applicable model. In the intermediate range, $3/2 \leq \sigma \leq 2$, $J(r)$ decays slower than r^{-5} and faster than $r^{-4.5}$, implying the system exhibits characteristics of different classes, with coefficients assuming intermediate values that depend on the value of σ .

We have used all possible combinations of n and d , and for each combination we look for the σ value so that the γ values are the same as determined by conventional methods. The values of α , σ , and β found for different pairs of n and d are given in Table 3.

In this case, $\sigma = 2.0$ is found, resulting in $J(r)$ spin interactions decayed as r^{-5} , which is a short-range spin interaction.

Table 3. The value of the critical coefficients with the different sets of d and n for the $\text{Sm}_2\text{Ni}_{17}$ alloy.

d	n	σ	ν	α	β	δ
3	1	2.0794	0.6665	0.00039	0.3068	5.5175
	2	1.9902	0.6964	−0.0892	0.3516	4.9419
	3	1.9376	0.7153	−0.1459	0.3799	4.6476
2	1	1.3717	1.0104	−0.0208	0.3174	5.3666
	2	1.3158	1.0532	−0.1065	0.3602	4.8468
	3	1.2828	1.0804	−0.1608	0.3874	4.5773
1	1	0.6819	2.0324	−0.0324	0.3232	5.2879
	2	0.6549	2.1162	−0.1162	0.3651	4.7961
	3	0.6389	2.1691	−0.1691	0.3915	4.5393

4. Conclusions

In this study, the purity and nature of the crystalline phase of the intermetallic compound $\text{Sm}_2\text{Ni}_{17}$ were verified by XRD coupled with Rietveld refinement, and the lattice parameters were determined. The measurement of the thermomagnetic properties shows that the studied compound passes from an ordered state to a disordered state when at temperatures equal to 160 K. The relative cooling power, maximum magnetic entropy change, and width at half-maximum of the magnetic entropy change are derived. The phenomenological model is found to agree with the experimental method. A rapid characterization of the magnetocaloric effect is possible with the derived phenomenological model. We investigated the critical behaviour of $\text{Sm}_2\text{Ni}_{17}$ near the transition temperature from the FM–PM state. Using the Banerjee criterion, this transition was found to be of the second-order. The critical coefficients β , δ , and γ were obtained from different techniques, the exponent $\beta = 0.25$ (KF) converges towards the value predicted by the tricritical MFM, while $\gamma = 1.39$ (KF) exhibits proximity to the value predicted by the 3D Heisenberg model. Using these exponents, the experimental data show a clear pattern of collapsing into two distinct curves, with one curve observed below T_C and the other above T_C . This behaviour suggests that the interactions are effectively re-normalized in a critical mode, in accordance with the scaling state equation. In our case, $\sigma = 2.0$ was found, resulting in a short-range spin interaction where $J(r)$ decayed as r^{-5} .

Author Contributions: Conceptualization, all authors; methodology, J.H., H.J. and K.N.; software, J.H., H.J. and K.N.; formal analysis, all authors; data curation, all authors; writing—original draft preparation, J.H. and H.J.; writing—review and editing, all authors. All authors have read and agreed to the published version of the manuscript.

Funding: This research received no external funding.

Institutional Review Board Statement: Not applicable.

Informed Consent Statement: Not applicable.

Data Availability Statement: Not applicable.

Acknowledgments: This work was supported by the “Centre National de la Recherche Scientifique (CNRS)”, France, by the “Ministère de l’Enseignement Supérieur et de la Recherche Scientifique” LMOP LR99ES17 Laboratory Tunis, LPA Laboratory Sfax, Tunisia, and by Qassim University.

Conflicts of Interest: The authors declare no conflicts of interest.

References

1. Giaque, W.F.; MacDougall, D.P. Attainment of Temperatures Below 1° Absolute by Demagnetization of $\text{Gd}_2(\text{SO}_4)_3 \cdot 8 \text{H}_2\text{O}$. *Phys. Rev.* **1933**, *43*, 768. [[CrossRef](#)]
2. Weiss, P.; Piccard, A. Le phénomène magnétocalorique. *J. Phys. Theor. Appl.* **1917**, *7*, 103–109. [[CrossRef](#)]
3. Nikitin, S.A.; Myalikgulyev, G.; Tishin, A.M.; Annaorazov, M.P.; Asatryan, K.A.; Tyurin, A.L. The magnetocaloric effect in $\text{Fe}_{49}\text{Rh}_{51}$ compound. *Phys. Lett. A* **1990**, *148*, 363–366. [[CrossRef](#)]
4. Pecharsky, V.K.; Gschneidner, K.A., Jr. Giant magnetocaloric effect in $\text{Gd}_5(\text{Si}_2\text{Ge}_2)$. *Phys. Rev. Lett.* **1997**, *78*, 4494. [[CrossRef](#)]

5. Pecharsky, V.K.; Gschneidner, K.A., Jr. Effect of alloying on the giant magnetocaloric effect of $\text{Gd}_5(\text{Si}_2\text{Ge}_2)$. *Phys. Rev. Lett.* **1997**, *167*, L179–L184. [\[CrossRef\]](#)
6. Gschneidner, K.A.; Pecharsky, V.K.; Brück, E.; Duijn, H.G.M.; Levin, E.M. Comment on “Direct Measurement of the ‘Giant’ Adiabatic Temperature Change in $\text{Gd}_5\text{Si}_2\text{Ge}_2$ ”. *Phys. Rev. Lett.* **2000**, *85*, 4190–4190. [\[CrossRef\]](#) [\[PubMed\]](#)
7. Tang, H.; Pecharsky, V.K.; Samolyuk, G.D.; Zou, M.; Gschneidner, K.A., Jr.; Antropov, V.P.; Schlagel, D.L.; Lograsso, T.A. Anisotropy of the Magnetoresistance in $\text{Gd}_5\text{Si}_2\text{Ge}_2$. *Phys. Rev. Lett.* **2004**, *93*, 237203. [\[CrossRef\]](#)
8. Tegus, O.; Fuquan, B.; Dagula, W.; Zhang, L.; Brück, E.; Si, P.Z.; De Boer, F.R.; Buschow, K.H.J. Magnetic-entropy change in $\text{Mn}_{1.1}\text{Fe}_{0.9}\text{P}_{0.7}\text{As}_{0.3-x}\text{Ge}_x$. *J. Alloys Compd.* **2005**, *396*, 6–9. [\[CrossRef\]](#)
9. Bartok, A.; Kuepferling, M.; Curcio, C.; Basso, V.; Pasko, A.; Zehani, K.; Bessais, L.; Mazaleyrat, F.; Lobue, M. Influence of particle size on the magnetocaloric properties of $\text{Mn}_{1.30}\text{Fe}_{0.65}\text{P}_{0.5}\text{Si}_{0.5}$ powders. In Proceedings of the 7th International Conference on Magnetic Refrigeration at Room Temperature (Thermag VII), Turin, Italy, 11–14 September 2016; Volume 400, pp. 333–338.
10. Bartok, A.; Kustov, M.; Cohen, L.F.; Pasko, A.; Zehani, K.; Bessais, L.; Mazaleyrat, F.; Lobue, M. Study of the first paramagnetic to ferromagnetic transition in as prepared samples of Mn–Fe–P–Si magnetocaloric compounds prepared by different synthesis routes. *J. Magn. Magn. Mater.* **2016**, *400*, 333–338. [\[CrossRef\]](#)
11. Pasko, A.; Bartok, A.; Zehani, K.; Bessais, L.; Mazaleyrat, F.; Lobue, M. X-ray diffraction analysis of the magnetoelastic phase transition in the Mn–Fe–P–Si magnetocaloric alloy. *AIP Adv.* **2016**, *6*, 056204. [\[CrossRef\]](#)
12. Dinesen, A.R.; Linderöth, S.; Mørup, S. Direct and indirect measurement of the magnetocaloric effect in $\text{La}_{0.67}\text{Ca}_{0.33-x}\text{Sr}_x\text{MnO}_{3\pm\delta}$. *J. Phys. Condens. Matter.* **2005**, *6*, 056204. [\[CrossRef\]](#)
13. Zhong, W.; Au, C.-T.; Du, Y.-W. Review of magnetocaloric effect in perovskite-type oxides. *Chin. Phys. B* **2013**, *22*, 057501. [\[CrossRef\]](#)
14. Felhi, H.; Smari, M.; Bajorek, Anna, Nouri, K.; Dhahri, E.; Bessais, L. Controllable synthesis, XPS investigation and magnetic property of multiferroic BiMn_2O_5 system: The role of neodymium doping. *Chin. Phys. B* **2019**, *29*, 198–209. [\[CrossRef\]](#)
15. Ameer, N.; Elleuch, F.; Triki, M.; Dhahri, E.; Bessais, L.; Hlil, E.K. Effect of A-site deficiency on the structural and magnetic properties of $\text{La}_{0.8-x}\text{Na}_{0.2-x}\text{MnO}_3$ oxides and estimation of the magnetocaloric behavior. *Solid State Commun.* **2019**, *29*, 198–209. [\[CrossRef\]](#)
16. Guo, D.; Moreno-Ramírez, L.M.; Law, J.Y.; Zhang, Y.; Franco, V. Excellent cryogenic magnetocaloric properties in heavy rare-earth based HfRENiGa_2 (HRE = Dy, Ho, or Er) compounds. *Sci. China Mater.* **2023**, *66*, 249–256. [\[CrossRef\]](#)
17. Zhang, Y.; Tian, Y.; Zhang, Z.; Jia, Y.; Zhang, B.; Jiang, M.; Wang, J.; Ren, Z. Magnetic properties and giant cryogenic magnetocaloric effect in B-site ordered antiferromagnetic $\text{Gd}_2\text{MgTiO}_6$ double perovskite oxide. *Acta Mater.* **2023**, *226*, 117669. [\[CrossRef\]](#)
18. Zhang, Y.; Xu, P.; Zhu, J.; Yan, S.; Zhang, J.; Li, L. The emergence of considerable room temperature magnetocaloric performances in the transition metal high-entropy alloys. *Mater. Today Phys.* **2023**, *32*, 101031. [\[CrossRef\]](#)
19. Zeng, Y.; Lu, Z.; Tang, N.; Li, X.; Zhao, R.W.; Yang, F.M. Structural, magnetic and microscopic physical properties of $(\text{Sm}, \text{Pr})_2\text{Fe}_{17}$ and their nitrides. *J. Magn. Magn. Mater.* **1995**, *139*, 11–18.
20. Younsi, K.; Russier, V.; Bessais, L. Structure and magnetic properties of nanocrystalline PrCo_3 compound. *J. Appl. Phys.* **2010**, *107*, 083916. [\[CrossRef\]](#)
21. Bouzidi, W.; Mliki, N.; Bessais, L. Structural and magnetic properties of new uniaxial nanocrystalline $\text{Pr}_5\text{Co}_{19}$ compound. *J. Magn. Magn. Mater.* **2017**, *441*, 566–571. [\[CrossRef\]](#)
22. Srinithi, A.K.; Sepehri-Amin, H.; Tang, X.; Tozman, P.; Li, J.; Zhang, J.; Kobayashi, S.; Ohkubo, T.; Nakamura, T.; Hono, K. Phase relations and extrinsic magnetic properties of Sm–(Fe,Co)–Ti–(Ga)-based alloys for ThMn_{12} -type permanent magnets. *J. Magn. Magn. Mater.* **2021**, *529*, 167866. [\[CrossRef\]](#)
23. Fujieda, S.; Fujita, A.; Fukamichi, K. Large magnetocaloric effect in $\text{La}(\text{Fe}_x\text{Si}_{1-x})_{13}$ itinerant-electron metamagnetic compounds. *App. Phys. Lett.* **2002**, *81*, 1276–1278. [\[CrossRef\]](#)
24. Fujieda, S.; Fujita, A.; Fukamichi, K. Relative cooling power of $\text{La}(\text{Fe}_x\text{Si}_{1-x})_{13}$ after controlling the Curie temperature by hydrogenation and partial substitution of Ce. *J. Magn. Magn. Mater.* **2007**, *310*, e1006–e1007. [\[CrossRef\]](#)
25. Boutahar, A.; Phejar, M.; Paul-Boncour, V.; Bessais, L.; Lassri, H. Theoretical work in magnetocaloric effect of $\text{LaFe}_{13-x}\text{Si}_x$ compounds. *J. Supercond. Nov. Magn.* **2014**, *27*, 1795–1800. [\[CrossRef\]](#)
26. Phejar, M.; Paul-Boncour, V.; Bessais, L. Investigation on Structural and Magnetocaloric Properties of $\text{LaFe}_{13-x}\text{Si}_x(\text{H,C})_y$ Compounds. *J. Solid State Chem.* **2016**, *16*, 95–102. [\[CrossRef\]](#)
27. Phejar, M.; Paul-Boncour, V.; Bessais, L. Structural and magnetic properties of magnetocaloric $\text{LaFe}_{13-x}\text{Si}_x$ compounds synthesized by high energy ball-milling. *Intermetallics* **2016**, *18*, 2301. [\[CrossRef\]](#)
28. Dan’Kov, S.Y.; Ivchenko, V.V.; Tishin, A.M.; Gschneidner, K.A.; Pecharsky, V.K. Magnetocaloric Effect in GdAl_2 and $\text{Nd}_2\text{Fe}_{17}$. *Adv. Cryog. Eng.* **2000**, *46*, 397–404.
29. Tishin, A.M.; Spichkin, Y.I. *The Magnetocaloric Effect and Its Applications*, 1st ed.; Institute of Physics Publishing: Bristol, UK, 2003; ISBN 9780429141379.
30. Mandal, K.; Yan, A.; Kerschl, P.; Handstein, A.; Gutfleisch, O.; Müller, K.H. The study of magnetocaloric effect in R_2Fe_{17} (R = Y, Pr) alloys. *J. Phys. D Appl. Phys.* **2004**, *37*, 2628. [\[CrossRef\]](#)
31. Chen, H.; Zhang, Y.; Han, J.; Du, H.; Wang, C.; Yang, Y. Magnetocaloric effect in R_2Fe_{17} (R = Sm, Gd, Tb, Dy, Er). *J. Magn. Magn. Mater.* **2008**, *320*, 1382–1384. [\[CrossRef\]](#)

32. Gorria, P.; Álvarez, P.; Marcos, J.S.; Llamazares, J.L.S.; Pérez, M.J.; Blanco, J.A. Crystal structure, magnetocaloric effect and magnetovolume anomalies in nanostructured $\text{Pr}_2\text{Fe}_{17}$. *Act. Mater.* **2009**, *57*, 1724–1733. [\[CrossRef\]](#)
33. Alvarez, P.; Gorria, P.; Franco, V.; Marcos, J.S.; Perez, M.J.; Sanchez-Llamazares, J.; Puente-Orench, I.; Blanco, J.J. Nanocrystalline $\text{Nd}_2\text{Fe}_{17}$ synthesized by high-energy ball milling: Crystal structure, microstructure and magnetic properties. *J. Phys. Condens. Mater.* **2010**, *22*, 216005. [\[CrossRef\]](#)
34. Saidi, M.; Nouri, K.; Walha, S.; Dhahri, E.; Kabadou, A.; Jemmali, M.; Bessais, L. Structural, Magnetic, Magnetocaloric and Mössbauer Spectrometry Study of $\text{Gd}_2\text{Fe}_{17-x}\text{Cu}_x$ ($x = 0, 0.5, 1$ and 1.5) Compounds. *J. Electron. Mater.* **2019**, *48*, 2242–2253. [\[CrossRef\]](#)
35. Bouzidi, W.; Nouri, K.; Bartoli, T.; Sedek, R.; Lassri, H.; Moscovici, J.; Bessais, L. Study of the magnetic and magnetocaloric properties at low-field in $\text{Nd}_2\text{Fe}_{17-x}\text{Si}_x$ intermetallics. *J. Magn. Magn. Mater.* **2020**, *497*, 166018 [\[CrossRef\]](#)
36. Carfagna, P.D.; Wallace, W.E. Magnetic Characteristics of 2–17 Lanthanide-Nickel Compounds. *J. Appl. Phys.* **1968**, *39*, 5259–5262 [\[CrossRef\]](#)
37. Zhong, X.P.; de Boer, F.R.; Jacobs, T.H.; Buschow, K.H.J. Magnetic coupling in rare-earth compounds of type R_2Ni_{17} . *J. Magn. Magn. Mater.* **1990**, *92*, 46–52 [\[CrossRef\]](#)
38. Moze, O.; Cadogan, J.M.; Kennedy, S.J.; Buschow, K.H.J. Magnetic order in R_2Ni_{17} intermetallics: A neutron-diffraction investigation. *Physica B* **2002**, *319*, 35–44 [\[CrossRef\]](#)
39. Banerjee, D.; Kumar, P.; Suresh, K.G.; Nigam, A.K. Anomalous magnetic and magnetocaloric properties of $\text{Er}_2\text{Ni}_{17}$. *J. Phys. D Appl. Phys.* **2007**, *40*, 2691–2694 [\[CrossRef\]](#)
40. Osterreicher, H.; Parker, F.T. Magnetic cooling near Curie temperatures above 300 K. *J. Appl. Phys.* **1984**, *55*, 4334. [\[CrossRef\]](#)
41. Jin, S.G.; Liu, L.M.; Wang, Y.L.; Chen, B.X. Research for room-temperature magnetic refrigerants in $\text{R}_x\text{Ce}_{2-x}\text{Fe}_{17}$ series. *J. Appl. Phys.* **1991**, *70*, 6275. [\[CrossRef\]](#)
42. Pawlik, K.; Skorvanek, I.; Kovac, J.; Pawlik, P.; Wyslacki, J.J.; Bodak, O.I. Phase structure and magnetocaloric effect in binary Pr–Fe alloys. *J. Magn. Magn. Mater.* **2006**, *304*, e510. [\[CrossRef\]](#)
43. Gschneidner, K.A., Jr.; Pecharsky, V.K.; Tsokol, A.O. Recent developments in magnetocaloric materials. *Rep. Prog. Phys.* **2005**, *68*, 1479. [\[CrossRef\]](#)
44. Mikheev, M.; Iwasieczko, W.; Platonov, S.P. The magnetocaloric effect in R_2Fe_{17} intermetallics with different types of magnetic phase transition. *Low Temp. Phys.* **2015**, *41*, 985.
45. Bessais, L.; Dorolti, E.; Djega-Mariadassou, C. High coercivity in nanocrystalline carbides $\text{Sm}(\text{Fe}, \text{Ga})_9$. *C. Appl. Phys. Lett.* **2005**, *87*, 192503. [\[CrossRef\]](#)
46. Khazzan, S.; Mliki, N.; Bessais, L.; Djega-Mariadassou, C. Rare-earth iron-based intermetallic compounds and their carbides: Structure and magnetic behaviors. *J. Magn. Magn. Mater.* **2010**, *322*, 224–229. [\[CrossRef\]](#)
47. Bensalem, R.; Tebib, W.; Alleg, S.; Sunol, J.J.; Bessais, L.; Greneche, J.M. Magnetic properties of nanostructured Fe_9P_8 powder mixture. *J. Alloys Compd.* **2009**, *471*, 24–27. [\[CrossRef\]](#)
48. Hamrita, A.; Slimani, Y.; Salem, M.K.B.; Hannachi, E.; Bessais, L.; Azzouz, F.B.; Salem, M.B. Superconducting properties of polycrystalline $\text{YBa}_2\text{Cu}_3\text{O}_{7-d}$ prepared by sintering of ball-milled precursor powder. *Ceram. Int.* **2014**, *40*, 1461–1470. [\[CrossRef\]](#)
49. Rietveld, H.M. Line profiles of neutron powder-diffraction peaks for structure refinement. *Acta Crystallogr.* **1967**, *22*, 151–152. [\[CrossRef\]](#)
50. Rietveld, H.M. A Profile Refinement Method for Nuclear and Magnetic Structures. *J. Appl. Crystallogr.* **1969**, *2*, 65–71. [\[CrossRef\]](#)
51. Rodríguez-Carvajal, J. Recent advances in magnetic structure determination by neutron powder diffraction. *J. Phys. B* **1993**, *192*, 55–69. [\[CrossRef\]](#)
52. Nouri, K.; Jemmali, M.; Walha, S.; Zehani, K.; Bessais, L.; Salah, A.B. The isothermal section phase diagram of the Sm–Fe–Ni ternary system at 800 °C. *J. Alloys Compd.* **2016**, *661*, 508–515. [\[CrossRef\]](#)
53. Pramanik, A.K.; Banerjee, A. Phase separation and the effect of quenched disorder in $\text{Pr}_{0.5}\text{Sr}_{0.5}\text{MnO}_3$. *J. Phys. Condens. Matter* **2008**, *20*, 275207. [\[CrossRef\]](#)
54. Li, Z.W.; Morrish, A.H. Negative exchange interactions and Curie temperatures for $\text{Sm}_2\text{Fe}_{17}$ and $\text{Sm}_2\text{Fe}_{17}$. *Phys. Rev. B* **1997**, *55*, 3670–3676. [\[CrossRef\]](#)
55. Foldeaki, M.; Chahine, R.; Bose, T.K. Magnetic measurements: A powerful tool in magnetic refrigerator design. *J. Appl. Phys.* **1995**, *77*, 3528–3537. [\[CrossRef\]](#)
56. Hamad, M.A. Theoretical work on magnetocaloric effect in $\text{La}_{0.75}\text{Ca}_{0.25}\text{MnO}_3$. *Adv. Ceram.* **2012**, *1*, 290–295. [\[CrossRef\]](#)
57. Griffith, L.D.; Mudryk, Y.; Slaughter, J.; Pecharsky, V.K. Material-based figure of merit for caloric materials. *J. Appl. Phys.* **2018**, *123*, 034902. [\[CrossRef\]](#)
58. Nouri, K.; Jemmali, M.; Walha, S.; Zehani, K.; Ben Salah, A.; Bessais, L. Structural, atomic Hirschfeld surface, magnetic and magnetocaloric properties of SmNi_5 compound. *J. Alloys Compd.* **2016**, *672*, 440–448. [\[CrossRef\]](#)
59. Fersi, R.; Bouzidi, W.; Mliki, N.; Bessais, L. Effect of stacking blocks on the low field magnetic refrigeration in nanocrystalline Pr_2Co_7 compound. *Intermetallics* **2018**, *100*, 181–187. [\[CrossRef\]](#)
60. Bouzidi, W.; Mliki, N.; Bessais, L. Second-Order Magnetic Transition and Low Field Magnetocaloric Effect in Nanocrystalline $\text{Pr}_5\text{Co}_{19}$ Compound. *J. Electron. Mater.* **2018**, *47*, 2776–2781. [\[CrossRef\]](#)

61. Sharma, M.K.; Kumar, A.; Kumari, K.; Park, S.J.; Yadav, N.; Huh, S.H.; Koo, B.H. Structural, Magnetic, and Magnetocaloric Studies of Ball-Milled $\text{Fe}_{100-x}\text{T}_x$ (T = Ni and Mn) Alloy. *Appl. Sci.* **2022**, *12*, 9098. [\[CrossRef\]](#)
62. Saidi, M.; Bessais, L.; Jemmali, M. Review of the influence of copper and chromium substitution on crystal structure, magnetic properties and magnetocaloric effect of $\text{GdFe}_{2-x}(\text{Cu}, \text{Cr})_x$ ($x = 0, 0.1, 0.15$ and 0.2) intermetallic compounds. *J. Phys. Chem. Solids* **2022**, *160*, 110343. [\[CrossRef\]](#)
63. Jaballah, H.; Charbonnier, V.; Bessais, L.; Mliki, N. Investigation of Spin Reorientation and Magnetocaloric Behavior in $\text{PrCo}_{5-x}\text{Cu}_x$ Compounds. *Mater. Res. Bull.* **2023**, *165*, 112326. [\[CrossRef\]](#)
64. Banerjee, B.K. On a generalised approach to first and second order magnetic transitions. *Phys. Lett.* **1964**, *2*, 16–17. [\[CrossRef\]](#)
65. Pramanik, A.K.; Banerjee, A. Critical behavior at paramagnetic to ferromagnetic phase transition in $\text{Pr}_{0.5}\text{Sr}_{0.5}\text{MnO}_3$: A bulk magnetization study. *Phys. Rev. B* **2009**, *79*, 214426 [\[CrossRef\]](#)
66. Arrott, A.; Noakes, J.E. Approximate equation of state for nickel near its critical temperature. *Phys. Rev. Lett.* **1967**, *19*, 786. [\[CrossRef\]](#)
67. Liu, Y.; Koch, R.J.; Hu, Z.; Aryal, N.; Stavitski, E.; Tong, X.; Attenkofer, K.; Bozin, E.S.; Yin, W.; Petrovic, C. Three-dimensional Ising ferrimagnetism of Cr-Fe-Cr trimers in FeCr_2Te_4 . *Phys. Rev. B* **2020**, *102*, 085158. [\[CrossRef\]](#)
68. Kouvel, J.S.; Fisher, M.E. Detailed magnetic behavior of nickel near its Curie point. *Phys. Rev.* **1964**, *136*, A1626. [\[CrossRef\]](#)
69. Fisher, M.E. The theory of equilibrium critical phenomena. *Rep. Prog. Phys.* **1967**, *30*, 615. [\[CrossRef\]](#)
70. Widom, B. Equation of state in the neighborhood of the critical point. *J. Chem. Phys.* **1965**, *43*, 3898–3905. [\[CrossRef\]](#)
71. Zhang, L.; Menzel, D.; Jin, C.; Du, H.; Ge, M.; Zhang, C.; Pi, L.; Tian, M.; Zhang, Y. Critical behavior of the single-crystal helimagnet MnSi . *Phys. Rev. B* **2015**, *91*, 024403. [\[CrossRef\]](#)
72. Jaballah, H.; Guetari, R.; Mliki, N.; Bessais, L. Magnetic properties, critical behavior and magnetocaloric effect in the nanocrystalline $\text{Pr}_2\text{Fe}_{16}\text{Al}$. *J. Phys. Chem. Solids* **2022**, *169*, 024403. [\[CrossRef\]](#)
73. Jaballah, H.; Nouri, K.; Mliki, N.; Bessais, L.; Jemmali, M. Universality class change from Mean-Field to 3D-Heisenberg in magnetocaloric compounds $\text{SmNi}_{3-x}\text{Fe}_x$. *Chem. Phys. Lett.* **2022**, *787*, 139260. [\[CrossRef\]](#)
74. Ma, Z.; Xu, P.; Ying, J.; Zhang, Y.; Li, L. Insight into the structural and magnetic properties of $\text{RECo}_{12}\text{B}_6$ (RE = Ce, Pr, Nd) compounds: A combined experimental and theoretical investigation. *Acta Mater.* **2023**, *247*, 118757. [\[CrossRef\]](#)
75. Fischer, S.F.; Kaul, S.N.; Kronmüller, H. Critical magnetic properties of disordered polycrystalline $\text{Cr}_{75}\text{Fe}_{25}$ and $\text{Cr}_{70}\text{Fe}_{30}$ alloys. *Phys. Rev. B* **2002**, *65*, 064443. [\[CrossRef\]](#)
76. Fisher, M.E.; Ma, S.K.; Nickel, B.G. Critical exponents for long-range interactions. *Phys. Rev. Lett.* **1972**, *29*, 917. [\[CrossRef\]](#)

Disclaimer/Publisher's Note: The statements, opinions and data contained in all publications are solely those of the individual author(s) and contributor(s) and not of MDPI and/or the editor(s). MDPI and/or the editor(s) disclaim responsibility for any injury to people or property resulting from any ideas, methods, instructions or products referred to in the content.